Ber. Ohara Inst. landw. Biol. 18 : 1-30 (1980)

TURBULENT TRANSFER OF WATER VAPOR OVER PADDY FIELDS

Keiji TAKEUCHI*, Eiji OHTAKI** and Takuro SEO

INTRODUCTION

Evapotranspiration from paddy fields was measured by the eddy correlation method. This method consists in measuring covariance $\overline{w'q'}$ in the atmospheric surface layer, where w is the vertical component of wind, and q is the specific humidity. The prime denotes the deviation from a mean, and the bar denotes a time average. A sonic anemometer was used for measuring w. A fine-wire thermocouple psychrometer and an infrared hygrometer were used for measuring q.

Two field experiments were made during September 1977. Using the data obtained, we demonstrate that our instrumentation provides a reasonably accurate estimate of $\overline{w'q'}$. Related statistical parameters, i. e., standard deviation $\sigma_q=\sqrt{\overline{q'^2}}$ and correlation coefficient r_{wq} between w' and q', are examined in the framework of the Monin-Obukhov similarity hypothesis. Spectral compositions of variance $\overline{q'^2}$ and covariance $\overline{w'q'}$ are analyzed by Tukey's procedure.

METHODS

Instrumentation

The vertical component of wind w was measured with a sonic anemometer (Kaijo Denki PA 112). Horizontal components u_x and u_y along two axes x and y crossed at right angle were measured with a "two-dimensional" sonic anemometer (Kaijo Denki PAS 211). The sensing path of the sonic anemometer is 20 cm in length.

Humidity was measured with two kinds of instrument constructed on different principles of hygrometry, i. e., a fine-wire thermocouple psychrometer and an infrared (IR) hygrometer.

Thermocouple psychrometer A copper-constantan thermocouple was used. The measuring junction was constructed by spot-welding wires of 0. 05 mmϕ. The thermocouple with the bare measuring junction was used as a dry-bulb thermometer. Its time constant was estimated as about 0. 05 sec for wind speeds of about 1 m/s.

The thermocouple with its measuring junction cotton-wound was used as a wet-bulb thermometer. Fig. 1 shows the psychrometer in its

* Present affiliation: Hokkaido District Office, Japan Weather Association, Sapporo.
** Present affiliation: College of Liberal Arts, Okayama University, Okayama.

field installation. The length of the cotton sheath is about 3 cm. A water reservoir feeds water to the wet-bulb through a cotton strand. The separation between the dry-bulb and the wet-bulb is about 1 cm.

The wetted cotton sheath significantly adds to the thermal inertia of the wet-bulb (Sano and Mitsuta, 1968). For our psychrometer, the

FIG. 1. Thermocouple psychrometer mounted in the middle of the sensor array of sonic anemometers. Over a paddy field on Sept. 3, 1977.

time constant of the wet-bulb τ_w was estimated from laboratory experiments to be about three times as large as the time constant of the dry-bulb τ_d.

The time constants τ_d and τ_w alone cannot specify the response characteristics of the psychrometer as a humidity sensor. It depends also on the temperature and humidity of the surroundings (Taylor, 1963). We examined the response of the psychrometer using the psychrometer equation written in terms of the fluctuating components:

$$q' = \left(\frac{c_p}{L} + \left. \frac{dq_s}{dT} \right|_{Tw} \right) T_w' - \frac{c_p}{L} T_d',$$

where T_d and T_w are the dry-bulb and the wet-bulb temperature, c_p is the specific heat of air at constant pressure, L is the latent heat of vaporization of water, and $\left. \frac{dq_s}{dT} \right|_{Tw}$ is the variation of saturation specific humidity with temperature at T_w.

It is assumed that inputs $T_d'(\omega)$ and $T_w'(\omega)$* are in phase or 180° out of phase, and the transfer function for $T_d'(\omega)$ and $T_w'(\omega)$ is

* $T_d'(\omega) = |T_d'(\omega)| \exp[j(\omega t - \phi_d(\omega)]$, $T_w'(\omega) = |T_w'(\omega)| \exp[j(\omega t - \phi_w(\omega)]$. $j = \sqrt{-1}$, ϕ is the phase angle, and ω is a particular frequency.

of the form $e^{-j\theta(\omega)}/\sqrt{1+\omega^2\tau^2}$, where $\theta(\omega)=\tan^{-1}(\omega\tau)$. It is assumed further that the amplitude ratio $|T_d'(\omega)|/|T_w'(\omega)|$ is constant and independent of frequency. Then, the amplitude ratio uniquely determines the Bowen ratio.

The Bowen ratio β is smaller than 1 over actively growing vegetation as is the case in the present study. Fig. 2 shows the results of calculation relevant to the present observation. Taylor's assumption $|T_d'(\omega)|/|T_w'(\omega)|=1$ corresponds to $\beta\simeq 0.3$.

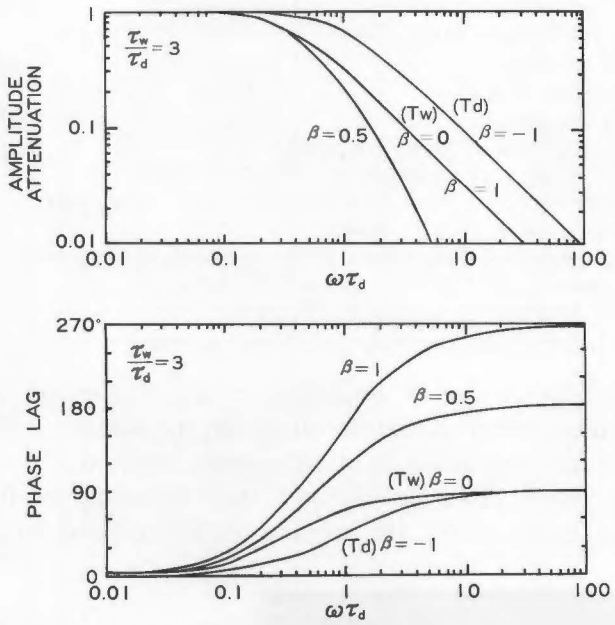

FIG. 2. Response characteristics of the thermocouple psychrometer.

τ_d: time constant of dry-bulb τ_w: time constant of wet-bulb
β: Bowen ratio ω: angular frequency

The curve labelled with $\beta=-1$ (T_d) represents performance of the dry-bulb; similarly, the curve $\beta=0$ (T_w) for the wet-bulb.

Fig. 2 shows that in the range $0<\beta<1$ the amplitude attenuation of q is greater than that of T_w and that the phase lag of the output of q relative to the input becomes significant in high frequencies. For a typical case with $\beta=0.5$ and $\tau_d=0.05$ sec the attenuation at frequency 1 Hz is 0.7 and the lag is 60°.

Infrared hygrometer We have developed an IR instrument for measuring fluctuations of atmospheric CO_2 concentration (Ohtaki and Seo, 1976). We showed that this instrument can be modified into a hygrometer by exchanging the optical filters (Seo and Ohtaki, 1976). The

latest model of the CO_2 instrument was used in the present observation. Table 1 shows specifications of the instrument. The primary improvement concerns raising the chopping frequencies of optical beams, thus enabling us to measure fluctuations of higher frequencies than with the earlier model.

TABLE 1
Specifications of infrared hygrometer

	Measurement	Reference
Radiation source: Inconell operated at 1000°K		
Optical transmission filter:		
Peak wavelength	2.6 μm	2.2 μm
Half-value width	0.079 μm	0.093 μm
Chopping frequency:	600 Hz	200 Hz
Sensing path length: 30 cm, adjustable		
Detector: PbSe, thermoelectrically cooled at −20°C		
Detectivity	1×10^{9} cm $Hz^{1/2}$ W^{-1} (typical)	
Time constant	10 μsec	
Cutoff frequency of electronics: 10 Hz, specified by lowpass filter		
Noise: approx. 0.12 g/kg rms in humidity value		
Operating sensitivity: approx. 0.3 V/g kg^{-1}		

The sensitivity of the IR hygrometer was determined in comparison with measurements with a thermocouple psychrometer. The results of the comparison are described in a subsequent section.

The noise value given in Table 1 was obtained as follows. The instrument is operated with its sensing path enclosed by a cylindrical

FIG. 3. Infrared hygrometer and sonic anemometer assembly over a wheat field on May 20, 1977.

cell filled with N_2 gas. The standard deviation of the output voltage measured in this operating condition is taken to represent noise.

The sensing path of the instrument was 30 cm in length. It was positioned vertical, parallel to the sonic path for measuring w. Fig. 3 illustrates the IR hygrometer installed by the side of the array of wind sensors.

Field experiments

Observation at Kurashiki Observation period: 1200–1639 JST, September 3, 1977. Site: paddy field of the experimental farm of the Institute for Agricultural and Biological Sciences, Kurashiki.

Fig. 4 shows the surface conditions around the observation point. The rice plants were at the growth stage of ear emergence. The crop

FIG. 4. Kurashiki site on Sept. 3, 1977. View toward southwest.

height was about 90 cm. The ground was covered by irrigation water to the depth of about 5 cm. The state of the sky was variable with clouds scattered or broken. The wind direction was southwest and the wind speed was moderate (1.5 to 2 m/s at 80 cm above the crop). The upwind fetch over the paddy field was about 90 m, interrupted by pathways and ditches.

Fig. 5 schematically shows the installation of the instruments. The limited fetch of the site restricted the measuring height to low levels.

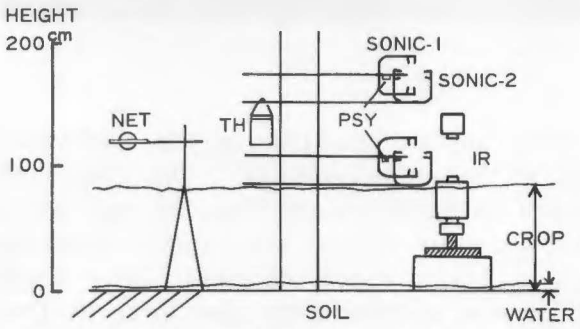

FIG. 5. Layout of the instruments at Kurashiki site on Sept. 3, 1977.

SONIC-1 : 1-dimensional sonic anemometer SONIC-2 : 2-dimensional sonic anemometer PSY : thermocouple psychrometer IR : infrared hygrometer NET : net radiometer TH : thermobottle containing cold junctions

The adopted heights were 110 cm and 170 cm above the ground. At these two heights we measured three components of wind velocity with sonic anemometers, and dry-bulb and wet-bulb temperatures with thermocouple psychrometers. These sensors were mounted on the ends of arms extending windward from the masts. The IR hygrometer was installed to measure humidity fluctuations over the 30 cm span centered around the height of 110 cm. The sensing path of the hygrometer was about 30 cm apart from the *w*-sensor. For reference, net radiation was measured with a Funk-type net radiometer.

Signals of the sensors were transmitted through cables of 100 m length to recorders housed in an observation hut. All signals were stored in two 7-channel data recorders. The output voltages of the thermocouples were amplified by 5,000 to be matched to the range of $\pm$1V of the data recorder.

Observation at Hachihama Observation period: 0000–2400 JST, September 18, 1977. Site: paddy field of the farm of Agricultural Faculty, Okayama University, situated at Hachihama.

FIG. 6. Hachihama site on Sept. 18, 1977. View toward north.

Fig. 6 shows the surface conditions of the observation point. The rice plants were at the milk-ripe stage. The crop height was about 70 cm. There was no flooding water, but the soil was saturated with water. The sky was clear through the period. Wind speeds were low (0.2 to 0.6 m/s at 215 cm above the crop). The wind direction was variable, though it was predominantly east to north from midnight to morning and south to southwest from early afternoon to evening. The upwind fetch over the experimental field exceeded 100 m in all sectors, but it was interrupted by paths; the shortest distance to the paths was about 20 m in the north direction. We mounted the instruments on the

arms extending eastwards from the masts.

Fig. 7 schematically shows the installation of the instruments. Measurements were taken at heights of 120 cm and 285 cm above the ground. At these two heights dry- and wet-bulb temperatures were measured with thermocouple psychrometers, and vertical components of wind were measured with sonic anemometers. Horizontal components of wind were

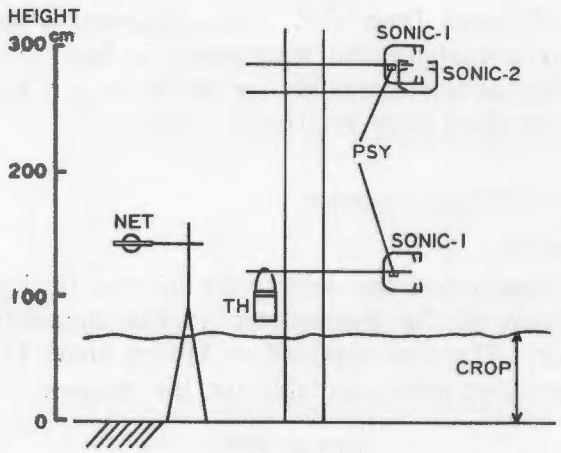

FIG. 7. Layout of the instruments at Hachihama site on Sept. 18, 1977.

For explanation of symbols, refer to the caption of Fig.5.

measured with a 2-dimensional sonic anemometer at 285 cm. The components u_x and u_y were synthesized by an analog device to give the wind direction and a scalar wind speed $u_s=\sqrt{u_x^2+u_y^2}$. These 7 elements (T_a, T_w and w at the two levels and u_s at the upper level) were recorded by a 7-channel data recorder. Wind direction and net radiation were recorded on a potentiometric recorder.

Data processing

Data recorded on analog tapes were digitized at the laboratory by an A/D converter at a sampling rate of 10 Hz. The A/D converters were preceded by lowpass filters with a cutoff frequency of 20 Hz; the filters were designed to effect reduction of 60 Hz line noise. The digital data were processed by a minicomputer (HP 2100).

We preliminarily divided the Kurashiki observation into successive runs of 6 min, and examined the time course of turbulence statistics on the basis of 6 min averages. For detailed analysis we selected 9 runs of 15 min duration during which the insolation remained relatively steady.

Similarly for the Hachihama observation, we preliminarily examined the diurnal course of turbulence statistics on the basis of 15 min averages. For further analysis we selected 20 runs of 10 to 16 min duration

during which the wind direction was relatively steady.

The selected runs* include no data obtained during the night. The fluctuations during the night were too small to warrant statistical analysis.

It is noted that in the Hachihama observation we recorded a scalar total wind speed $u_s=\sqrt{u_x^2+u_y^2}$ instead of the streamwise component u of the horizontal wind. Mitsuta *et al.* (1973) showed that u_s is greater than u and that $\overline{u_s'w'}$ can be different from $\overline{u'w'}$. The difference is not negligible when wind direction is variable and wind speed is low. We assumed that u_s may be treated as approximately equal to u for the selected periods when wind directions were relatively steady.

RESULTS AND DISCUSSIONS

Standardization of IR hygrometer

As mentioned above, we determined the sensitivity of the IR hygrometer by referring the output of the hygrometer to the humidity measured by the psychrometer. The data obtained at 110 cm above the ground in the Kurashiki observation were available for the purpose.

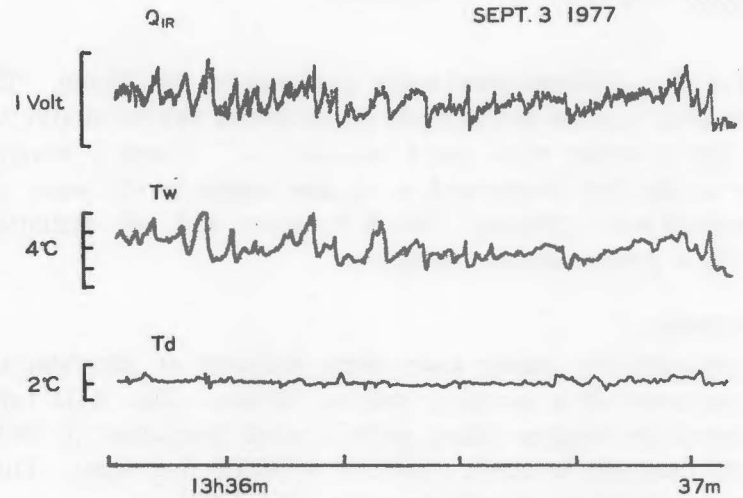

FIG. 8. Example of analog records of the output of the IR hygrometer (Q_{IR}) and wet- and dry-bulb temperatures measured with a thermocouple psychrometer (T_w and T_d).
From measurement at a height of 20 cm above the crop at Kurashiki on Sept. 3, 1977.

Fig. 8 shows analog records of the dry-bulb and wet-bulb temperatures measured with the psychrometer and the output of the IR hygrometer. In this selected but typical example in the Kurashiki obser-

* The date of the selected runs, 29 in total, are available on request to the authors.

vation, the wet-bulb temperature shows large fluctuations while the air temperature shows very small fluctuations. The fluctuations of the IR hygrometer output are similar to those of wet-bulb temperature. The psychrometer equation ensures that in these conditions the fluctuations of wet-bulb temperature approximate the humidity fluctuations.

The similarity in the frequency domain was examined by the coherency between the specific humidity measured with the psychrometer and the output of the IR hygrometer. Fig. 9 shows the results of calculation for the selected period 1331 to 1352. The coherency is greater

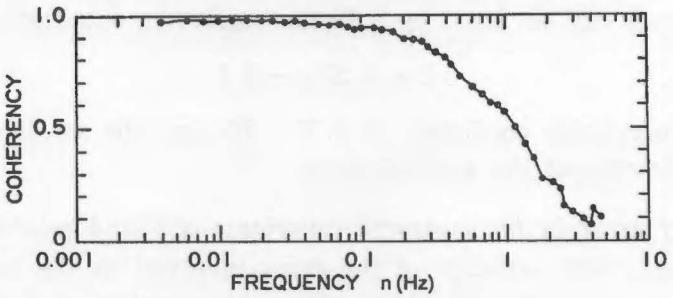

FIG. 9. Coherency between humidity fluctuations measured with thermocouple psychrometer and IR hygrometer.

Based on measurements at a height of 20 cm above the crop at Kurashiki during 1331–1352 JST on Sept. 3, 1977.

Coherency is defined by $\sqrt{(Co(n)^2+Q(n)^2)/S_x(n)S_y(n)}$, where $S_x(n)$ and $S_y(n)$ are power spectra of time series x and y, and $Co(n)$ and $Q(n)$ denote cospectrum and quadrature spectrum between x and y.

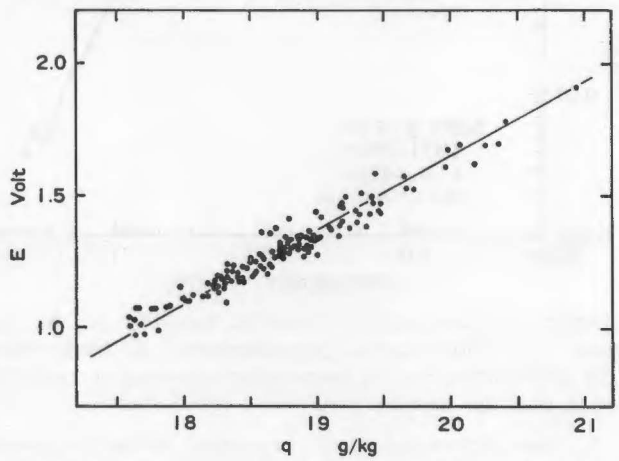

FIG. 10. Relation between output of IR hygrometer (E) and specific humidity (q) measured with thermocouple psychrometer.

Based on measurements at a height of 20 cm above the crop at Kurashiki during 1335–1350 JST on Sept. 3, 1977.

than 0.9 in the low frequency range below 0.2 Hz. The decrease in coherency at higher frequencies is due to the difference in frequency response between the instruments.

For standardization of the IR hygrometer we selected data in the period 1335 to 1350. During this 15 min period the humidity fluctuations were large in amplitude and the trend was not significant. Taking into account the results of coherence analysis, we used for comparison the average values from 72 digital data sampled at the interval of 0.1 sec. Fig. 10 shows the output E (Volt) of the IR hygrometer plotted against the specific humidity q (g/kg) obtained with the psychrometer. The measurements can be fitted by a linear regression equation:

$$E = 0.27\,q - 3.7$$

with the correlation coefficient of 0.97. We use the sensitivity 0.27V/(g kg^{-1}) throughout the present study.

Estimate of error in the measured covariance $\overline{w'q'}$ and related statistics

We begin with estimate of the error involved in the measurement of power spectra. Fig. 11 shows the power spectra of humidity fluc-

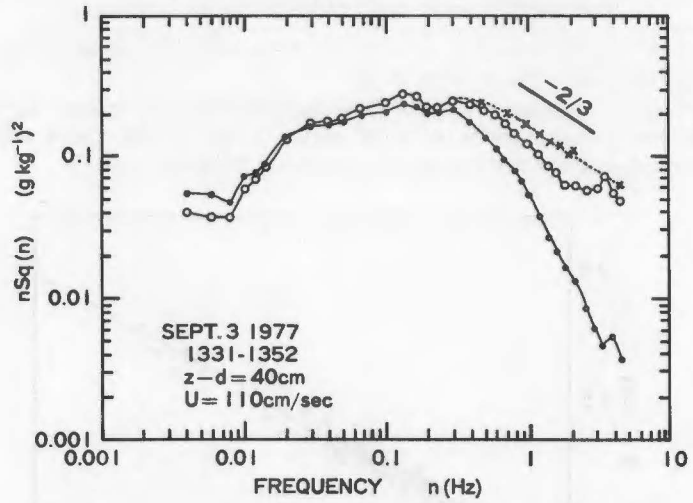

FIG. 11. Power spectrum nS_q (n) of specific humidity q. ●: from measurement with thermocouple psychrometer; ○: from measurement with IR hygrometer; x: IR hygrometer spectrum corrected for space averaging over the sensing path.

U: mean horizontal wind z: height above the ground
d: zero-plane displacement
σ_q^2(PSY)=0.88(g/kg)² σ_q^2(IR)=1.08(g/kg)²
IR hygrometer spectrum ceases to drop beyond 2 Hz.
This results from the aliasing effect. The high frequency end of the corrected spectrum represents an extrapolation by the −2/3 power law.

tuations $S_q(n)$ multiplied by frequency n. The selected period is the same as that used in coherence analysis for standardization of the IR hygrometer. The IR hygrometer spectrum is affected by underestimate in high frequencies due to space averaging of fluctuations over the sensing path. We corrected the q-spectrum for this averaging effect by using the spectral transfer function computed by Gurvich-Silverman for scalar variables (Silverman, 1968). The corrected power spectrum represented by crosses in Fig. 11 follows on the high frequency side the $-2/3$ power law for the inertial subrange. Evaluating variance $\overline{q'^2}=\int_{f_L}^{f_H} S_q(n)dn$ from the corrected and the uncorrected spectra, we assessed the underestimate in variance $\overline{q'^2}$ from the IR hygrometer to be about 15 %. In the above integral the limiting frequencies f_H and f_L are specified by averaging time and sampling rate, respectively.

Variance $\overline{w'^2}=\int_{f_L}^{f_H} S_w(n)dn$ is also affected by underestimate due to space averaging over the sonic path (20 cm). We corrected the measured w-spectrum for this effect using the transfer function given by Kaimal *et al.* (1968) for vector fields. The result showed that the underestimate in variance $\overline{w'^2}$ was about 15 %.

Fig. 12 shows w-q cospectra $Co_{wq}(n)$ in the same period as for the power spectra. In the coordinates adopted: nCo_{wq} vs. log n, the area

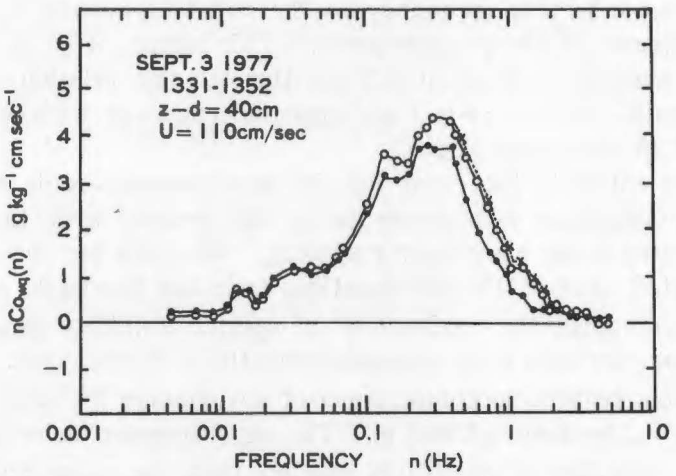

FIG. 12. Cospectrum $nCo_{wq}(n)$ of vertical wind w and specific humidity q. ●: from measurement with psychrometer and sonic anemometer assembly; ○: from measurement with IR hygrometer and sonic anemometer assembly; x: IR cospectrum corrected for space averaging over the sensing path.

$\overline{w'q'}$(PSY)=9.21(g/kg·cm/s) $\overline{w'q'}$(IR)=10.66(g/kg·cm/s)

under the curve over a frequency interval Δn is proportional to the spectral contribution to covariance, $Co_{wq}(n)\Delta n$. The crosses in Fig. 12 show the cospectrum from the sonic anemometer–IR hygrometer system corrected for space averaging of w' and q'. The cospectral transfer function was taken as the product of transfer functions for w' and q'. Comparing the areas under the curves representing the corrected and uncorrected spectrum, we find that the underestimate in covariance is about 3 %.

With the estimates given above, the effect of space averaging on the correlation coefficient r_{wq} is determined as follows:

$$r_{wq}=\overline{w'q'}/\sigma_w\sigma_q=\frac{0.97}{(0.85)^{1/2}\ (0.85)^{1/2}}=1.14$$

or 14 % overestimate.

Fig. 11 shows that the power spectrum of q derived from the psychrometer data has a shape similar to that derived from the IR hygrometer data at frequencies lower than about 0.1 Hz. At higher frequencies the spectral density computed from the psychrometer data falls more steeply than that computed from the IR hygrometer data. This high frequency loss makes the variance measured with the psychrometer smaller than that measured with the IR hygrometer.

Fig. 11 shows also that the density of the psychrometer spectrum is 1/2 of the corrected IR hygrometer spectrum at a frequency $n\simeq 0.6$ Hz. We can take this frequency as the cutoff frequency f_c in the frequency response of the psychrometer. This value of f_c is equivalent to a time constant τ of about 0.3 sec through the relation $\tau=1/(2\pi f_c)$ (e. g., Pasquill, 1974). $\tau=0.3$ sec appears consistent with $\tau_d=0.05$ sec and $\tau_w=0.15$ sec given above.

We can estimate the error for the psychrometer–sonic anemometer system by comparing measurements by this system with those by the IR hygrometer–sonic anemometer system. We used for the comparison the 9 selected runs of 15 min durations from the Kurashiki observation. Fig. 13(a) compares the variance $\overline{q'^2}$ of specific humidity measured with the psychrometer with that measured with the IR hygrometer. Fig. 13(b) and (c) show respective comparisons of covariances $\overline{w'q'}$ and correlation coefficients r_{wq} between w' and q'. The psychrometer value of variance of specific humidity $\overline{q'^2}$ was 20 % smaller than the value obtained with the IR hygrometer. The psychrometer–sonic anemometer system gave the value of covariance $\overline{w'q'}$ 10 % smaller than the value obtained by the IR hygrometer–sonic anemometer system. The correlation coefficient r_{wq} given by the psychrometer–sonic anemometer system was about 8 % smaller than that given by the IR hygrometer–sonic anemometer system.

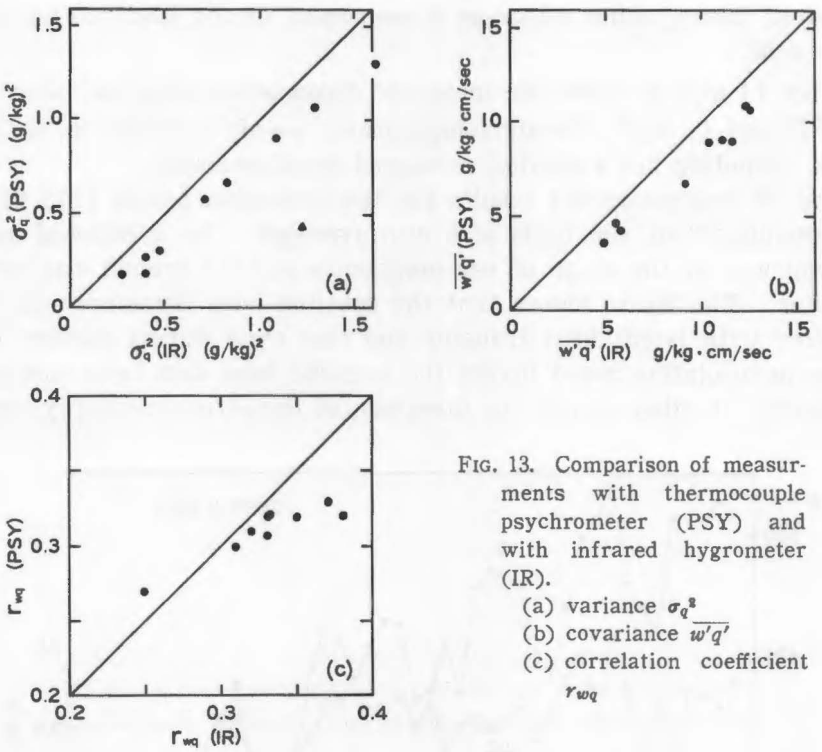

FIG. 13. Comparison of measurments with thermocouple psychrometer (PSY) and with infrared hygrometer (IR).
(a) variance σ_q^2
(b) covariance $\overline{w'q'}$
(c) correlation coefficient r_{wq}

Based on measurements at a height of 20 cm above the crop at Kurashiki on Sept. 3, 1977. Averaging time: 15 min.

From these comparisons and the estimated errors for the IR hygrometer–sonic anemometer system, we can estimate the error introduced in the psychrometer–sonic anemometer system.

The errors estimated above are summarized in the following table (+ overestimate, − underestimate).

	σ_q^2	r_{wq}	$\overline{w'q'}$	σ_w^2
	(%)			
IR hygrometer + sonic anemometer	−15	+14	− 3	−15
thermocouple psychrometer + sonic anemometer	−32	+ 5	−22	−15

It is noted that these estimates apply at a height of about 20 cm above tall crops for wind speeds of about 1 m/s and near-neutral stratification. If the fetch requirement allowed measurements to be taken at greater height, the errors discussed here would have been reduced.

Turbulent flux of water vapor as a component of the heat balance of the paddy field

Figs. 14 and 15 show the measured fluxes of sensible and latent heat $c_p\rho\ \overline{w'T'}$ and $L\rho\ \overline{w'q'}$ (T=air temperature, ρ=air density) in the time course, including net radiation measured simultaneously.

Fig. 14 represents the results for the afternoon period 1215 to 1630 on September 3 on the basis of 6 min averages. As mentioned above, the crop was at the stage of ear emergence and the ground was covered by water. The figure shows that the sensible heat transfer was small compared with latent heat transfer and that even during midday hours a drop in insolation could invert the sensible heat flux from upward to downward; in other words, an inversion of temperature readily appears

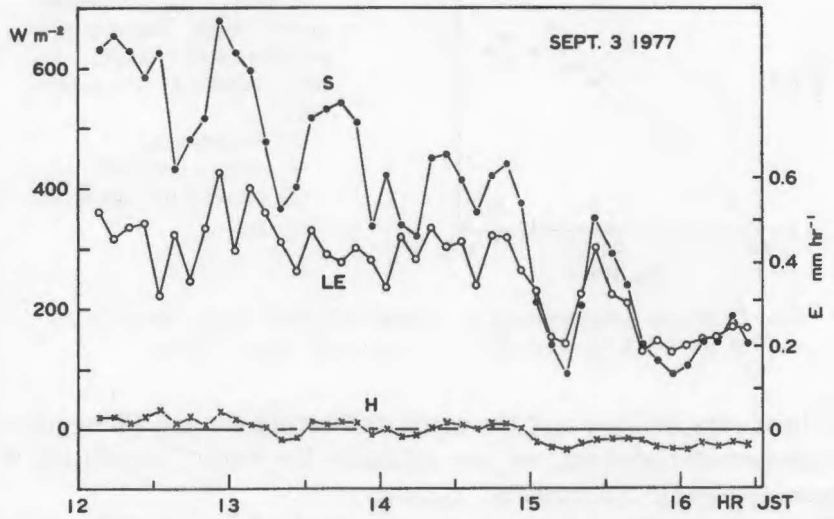

FIG. 14. Variation of heat balance components during afternoon over a paddy field at the stage ear emergence. Kurashiki, Sept. 3, 1977.

S: net radiation LE: latent heat flux
H: sensible heat flux E: evapotranspiration
LE represents the measurement with IR hygrometer-sonic anemometer system.

over the paddy. The paddy field transferred heat to the overlying air almost exclusively through evapotranspiration. The evapotranspiration was maintained at a high rate of about 0.7 mm/hr from 1200 to 1500. The variation in evapotranspiration was primarily associated with variation in net radiation, though it was superposed by minor variations difficult to explain. The latent heat transfer averaged more than 60% of net radiation received by the paddy field.

Fig. 15 represents the full diurnal course of sensible and latent heat fluxes and net radiation on the basis of 15 min averages for September 18. In this period the crop was at the milk-ripe stage and the soil surface was exposed without flooding water. Evapotranspiration still played the predominant part in daytime heat transfer from the paddy field to air, but its importance was somewhat diminished and sensible heat transfer became active, particularly in the forenoon.

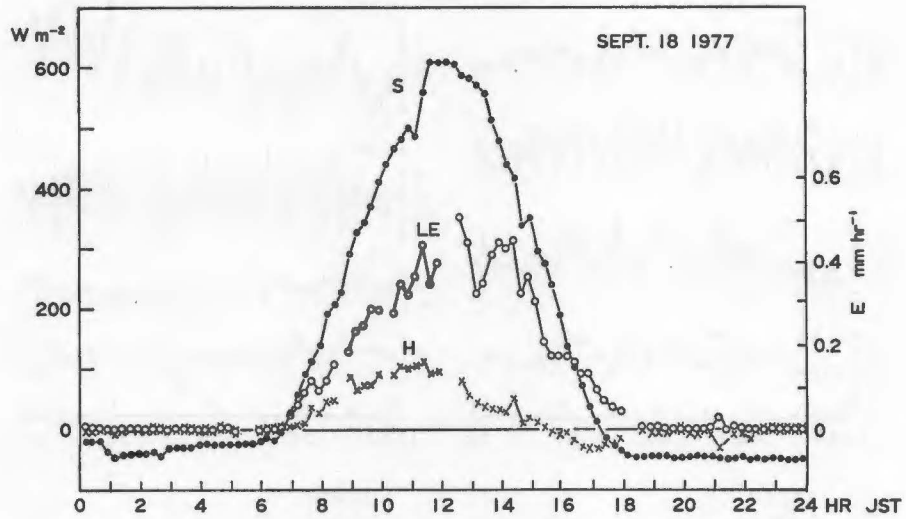

FIG. 15. Diurnal variation of heat balance components over a paddy field at milk ripe stage. Hachihama, Sept. 18, 1977.

S: net radiation LE: latent heat flux
H: sensible heat flux E: evapotranspiration

LE and H represent the averages from measurements at two heights 120 and 285 cm above the ground.

Both observations revealed that there is a period in the evening during which sensible heat flux is downward while latent heat flux continues to be upward.

The total amount of evapotranspiration was 1.8 mm for the afternoon period 1215 to 1630 on September 3, and 2.6 mm for the daytime period 0600 to 1900 on September 18. The evapotranspiration from the paddy field in the actively growing stage of the crop has been estimated from heat balance to be 3 to 4 mm in daytime total (Seo and Yamaguchi, 1968). The present results show that the estimate by the heat balance method is compatible with the estimate by the eddy correlation technique.

Turbulent fluctuations in the surface layer above the paddy field

Figs. 16 and 17 show segments of the analog records of turbulent fluctuations observed at Hachihama on September 18. Fig. 16 illustrates an unstable case, and Fig. 17 illustrates a near-neutral (slightly stable) case.

Unstable case. (09 h 48 m–52 m) Air temperature T_a and wet-bulb temperature T_w at the 285 cm level exhibited very similar fluctuations

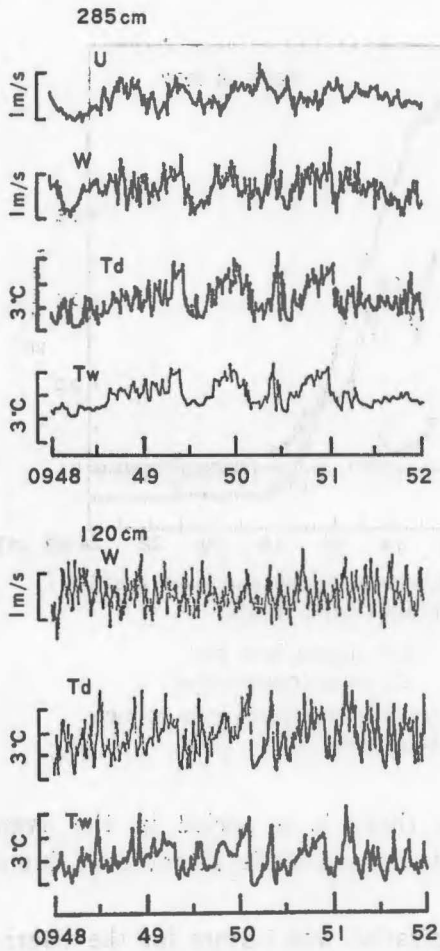

FIG. 16

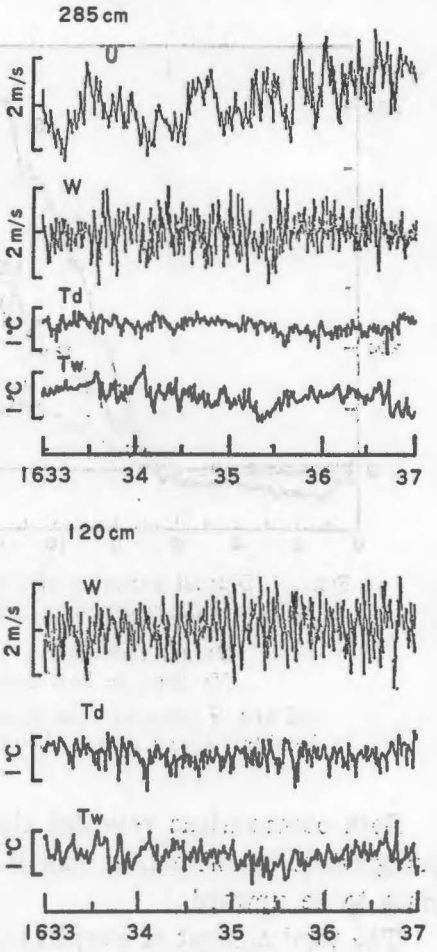

FIG. 17

FIG. 16. Example of records of turbulent fluctuations over a paddy field. Unstable case. Hachihama, Sept. 18, 1977.

U: horizontal wind speed W: vertical component of wind
T_a: air temperature T_w: wet-bulb temperature

FIG. 17. Example of records of turbulent fluctuations over a paddy field. Near-neutral (slightly stable) case. Hachihama, Sept. 18, 1977.

The symbols are the same as in Fig. 16.

with positive correlation, though the T_w-trace appears smoothed by greater instrumental inertia of the wet-bulb. The fluctuations of vertical wind w also broadly follow temperature fluctuations.

It is remarkable that in addition to short-period random fluctuations, relatively slow variations characterized by gradual rise and sharp drop, appeared in the intervals of the order of 1/2 min. These variations are considered to represent buoyant "plumes" described by Webb (1965) and demonstrated by Kaimal and Businger (1970).

At the lower 120 cm level, the correlation between T_a- and T_w-fluctuations is still well-defined, though high frequency fluctuations become more pronounced. The similarity of w- fluctuations and temperature fluctuations becomes less distinct.

Near-neutral case (16 h 33 m–37 m) Compared with the unstable case, high frequency fluctuations are more prevalent at the heights of both 285 and 120 cm, and the difference in frequency compositions between these two heights is less distinct. The fluctuations of T_a and T_w are diminished in amplitude, compared with those in the unstable case.

The T_a- and T_w- fluctuations are negatively correlated. The correlation is more evident at the lower level. The T_a- fluctuations are asymmetrical, such that temperature rises are suppressed. This feature results in negative skewness in the probability distribution of T_a- fluctuations.

It is noted that T_a- and T_w- fluctuations are of the same order of magnitude in either case. The psychrometer equation implies that q-fluctuations are positively correlated with T_w- fluctuations in these conditions.

Application of Monin-Obukhov similarity theory

Inspection of the records has indicated some salient features of the turbulent fluctuations. We proceed to analyze the turbulence statistics on the basis of the Monin-Obukhov similarity theory.

Turbulent fluxes of momentum, heat and water vapor are defined:

$$\tau/\rho = \overline{-w'u'},$$
$$H/c_p\rho = \overline{w'T'},$$
$$E/\rho = \overline{w'q'}$$

The fluxes are assumed to be constant with height for $z-d \gg z_0$ in the atmospheric surface layer, where z is the height above the ground, d is the zero-plane displacement and z_0 is the roughness length.

The Monin-Obukhov similarity theory predicts that any turbulence statistics can be scaled by scaling parameters $u_* = (\overline{-w'u'})^{1/2}$, $T_* =$

$-\overline{w'T'}/u_*$, $q_*=-\overline{w'q'}/u_*$, $L_\theta=\dfrac{u_*^2T}{gkT_*}$, and $z-d$. Here g is the acceleration of gravity and $k=0.4$ is the von Kármán constant. In particular, $\sigma_w=\sqrt{\overline{w'^2}}$ is expressed in the form

$$\frac{\sigma_w}{u_*}=\phi_1\left(\frac{z-d}{L_\theta}\right),$$

where ϕ_1 is a universal function and $\zeta=(z-d)/L_\theta$ is a stability parameter. ζ is replaced by $\zeta_v=(z-d)/L$ in the present study, where $\dfrac{1}{L}=\dfrac{1}{L_\theta}+\dfrac{1}{L_q}$. The term $\dfrac{1}{L_q}$ takes into account the effect of vapor flux on the density fluctuations with $L_q=\dfrac{u^{*2}T_v}{0.61\,gkq_*T}$, where T_v is the virtual temperature (Busch, 1973).

The zero-plane displacement d was derived for the Kurashiki observation from wind measurements at levels of 110 cm and 170 cm above the ground. The logarithmic law of the wind profile was applied in the derivation, since stratification during this period was near-neutral with ζ_v varying between -0.02 and $+0.02$ at 170 cm above ground. The evaluation gave $d=70$ cm. The crop height h was about 90 cm, thus $d/h\simeq 0.8$. In the Hachihama observation, wind measurements were available only at one height, 285 cm above ground. We assumed the ratio d/h obtained at Kurashiki as valid for the Hachihama observation. The crop height of 70 cm gives $d=55$ cm.

The Kurashiki data give the roughness length $z_0=8$ cm with $d=70$ cm. The value of z_0 for the Hachihama observation is assumed as 6 cm. With the values of z, d and z_0 given above, the approximate values of $(z-d)/z_0$ are as follows:

	z cm	$(z-d)/z_0$
Kurashiki	170	12
($d=70$, $z_0=8$)	110	5
Hachihama	285	38
($d=55$, $z_0=6$)	120	10

Comparison of turbulent fluxes at two heights

The Monin-Obukhov similarity is valid within the constant flux layer near the ground surface. The extent to which this prerequisite is satisfied in our observations can be checked by comparing the fluxes measured at two heights. The height range covered is 20 to 80 cm above the crop for the Kurashiki observation and 50 to 215 cm above the crop for the Hachihama observation. The values $(z-d)/z_0$ have been given above.

A comparison of the momentum fluxes was feasible only for the Kurashiki observation. Fig. 18 shows that the momentum flux exhibits no systematic deviation from the constancy of flux.

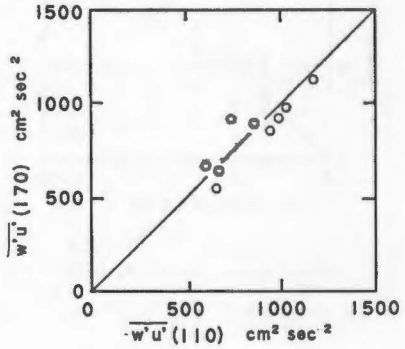

FIG. 18. Comparison of turbulent fluxes of momentum between two heights 110 cm and 170 cm above the ground. Kurashiki, Sept. 3, 1977. Crop height: 90 cm.

The 1:1 line in Figs. 18 to 20 is entered for reference purpose.

Figs. 19 (a) and (b) show that the same applies approximately to the flux of water vapor, though the Hachihama observation indicates some evidence of decrease in vapor flux with height.

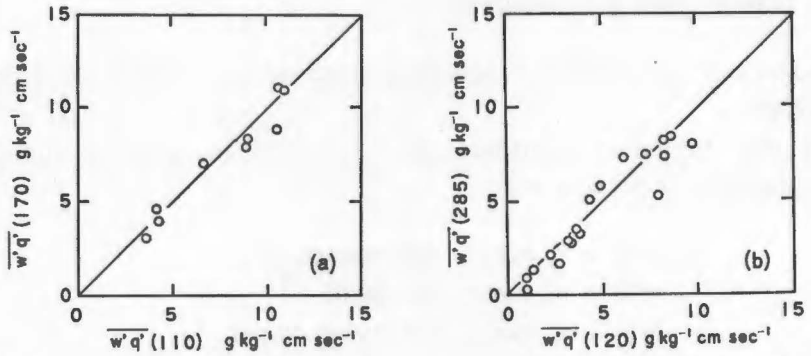

FIG. 19. Comparison of turbulent fluxes of water vapor between two heights.
(a) Kurashiki, Sept. 3, 1977. Measuring height: 110 and 170 cm above the ground. Crop height: 90 cm.
(b) Hachihama, Sept. 18, 1977. Measuring height: 120 and 285 cm above the ground. Crop height: 70 cm.

Psychrometer value of q' was used in evaluating $\overline{w'q'}$.

Figs. 20 (a) and (b) show that there was considerable difference in heat fluxes between two heights. In particular, the Hachihama data indicate that the heat flux systematically decreased in magnitude with increasing height; the difference between the two heights was about 20 % on the average.

In spite of some evidence of flux divergence, we supposed that it was not so serious as to invalidate application of the similarity theory.

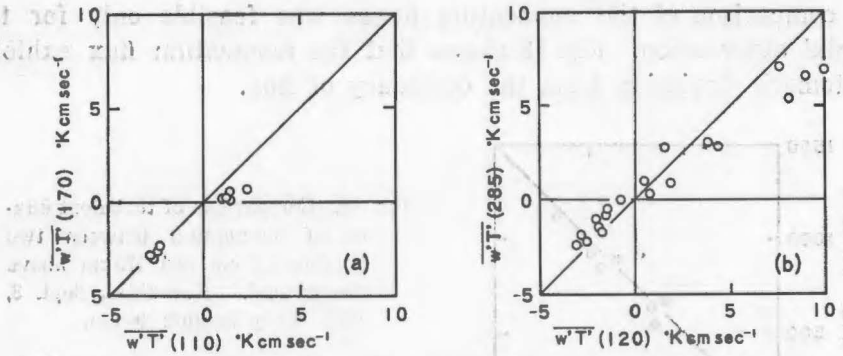

FIG. 20. Comparison of turbulent heat fluxes between two heights.
(a) Kurashiki, Sept. 3, 1977 (b) Hachihama, Sept. 18, 1977
Specifications of the height are the same as in Fig. 19.

It is noted in this context that turbulence statistics at each height were scaled by local values of parameters, i. e., parameters calculated using fluxes measured at respective heights. There is one exception: to the momentum flux at the lower level at Hachihama, the value measured at the higher level was assigned.

Characteristics of turbulent statistics involved in vertical turbulent transport

Vertical turbulent transport can be written in terms of correlation r and standard deviation σ:

$$\overline{w'u'} = r_{uw}\sigma_u\sigma_w \quad \text{for momentum,}$$
$$\overline{w'T'} = r_{wT}\sigma_w\sigma_T \quad \text{for heat,}$$
$$\overline{w'q'} = r_{wq}\sigma_w\sigma_q \quad \text{for water vapor.}$$

It is noted that psychrometer values of q are used in the following analysis. It is further noted that the Kurashiki data covers a narrow range of ζ_v near the neutral stratification (-0.02 to $+0.02$) and they are appropriately grouped for graphical representation in this section.

Standard deviation Fig. 21 (a) shows the normalized standard deviation of specific humidity $\sigma_q/|q_*|$ as a function of the stability parameter ζ_v. The values of σ_q are underestimated, as discussed in the previous section. The underestimate in σ_q is partly compensated by the underestimate in q_*.

The figure shows that the ratio $\sigma_q/|q_*|$ decreases with increasing instability. The equation

$$\sigma_q/|q_*| = a_E(-\zeta_v)^{-1/3}$$

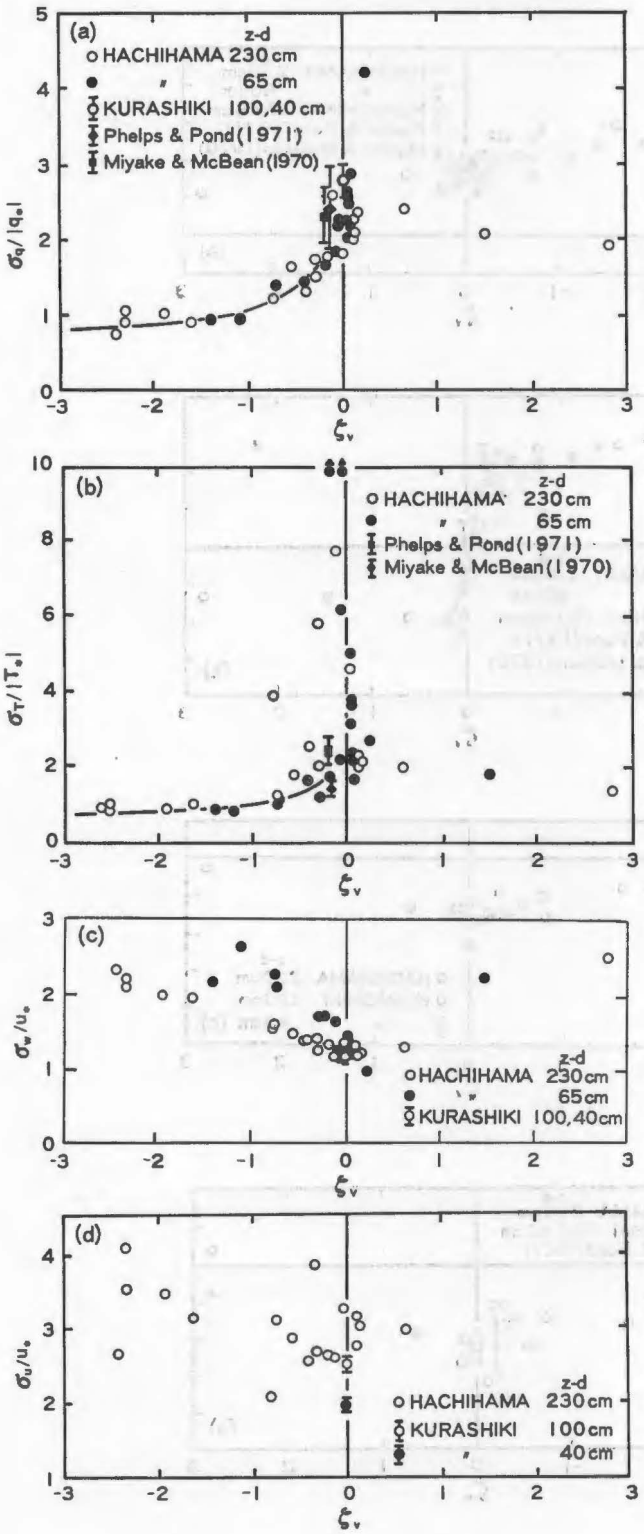

FIG. 21. Normalized standard deviation as a function of stability parameter ζ_v.
(a) specific humidity $\sigma_q/|q_*|$
(b) air temperature $\sigma_T/|T_*|$
(c) vertical component of wind σ_w/u_*
(d) horizontal wind σ_u/u_*

The arrow attached to data point indicates an off-scale value.

Remarks: (1) The curve entered in Fig. 21(a) is the empirical curve $\sigma_q/|q_*| = 1.1(-\zeta_v)^{-1/3}$ valid for $\zeta_v < -0.2$. The curve of the same functional form is drawn for reference in Fig. 21(b). (2) In Fig. 21(b) Kurashiki data are not entered because of the large variability. They are listed below in average values from 9 runs.

z-d(cm)	100§	40
ζ_v	0.0012 ±0.016	−0.00023 ±0.0055
$\sigma_T/\|T_*\|$	6.8±5.7	5.1±1.7

§ 3 data for which $|T_*| < 0.01$ were rejected.

(3) u is the longitudinal component for Kurashiki data and the total wind speed for Hachihama data.

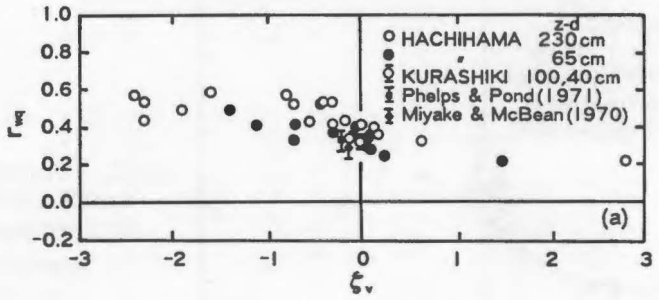
z-d
HACHIHAMA 230cm
" 65cm
KURASHIKI 100,40cm
Phelps & Pond(1971)
Miyake & McBean(1970)
(a)
r_{wq}
ζ_v

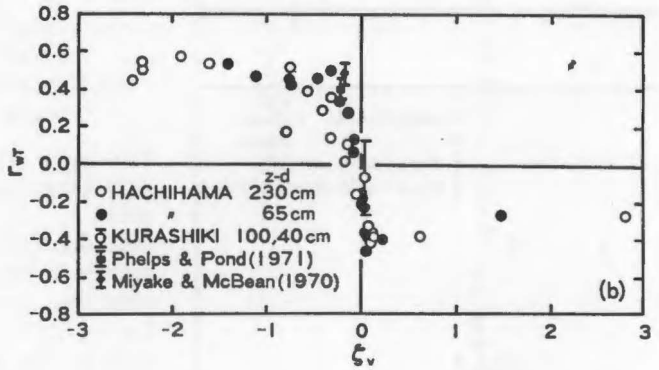
z-d
HACHIHAMA 230cm
" 65cm
KURASHIKI 100,40cm
Phelps & Pond(1971)
Miyake & McBean(1970)
(b)
r_{wT}
ζ_v

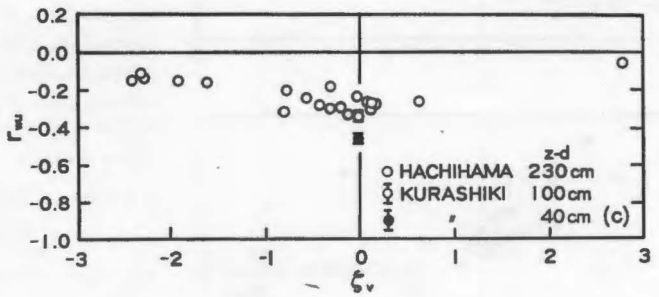
z-d
HACHIHAMA 230cm
KURASHIKI 100cm
" 40cm
(c)
r_{wu}
ζ_v

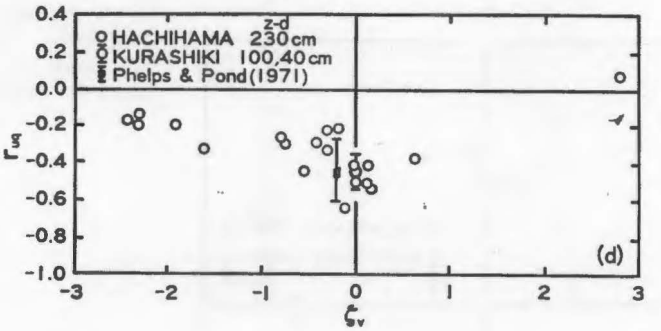
z-d
HACHIHAMA 230cm
KURASHIKI 100,40cm
Phelps & Pond(1971)
(d)
r_{uq}
ζ_v

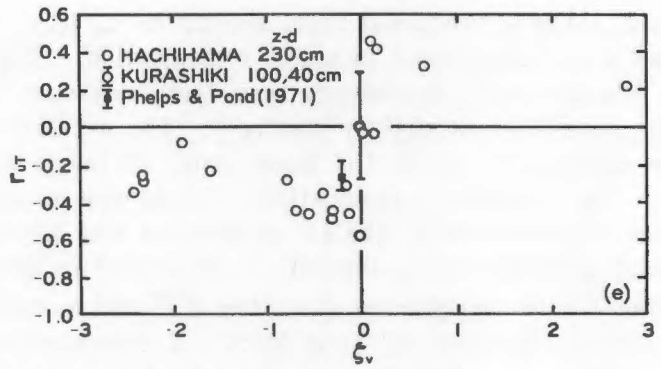

FIG. 22. Correlation coefficient as a function of stability parameter ζ_v between (a) w and q, (b) w and T, (c) w and u, (d) u and q, and (e) u and T.

q: specific humidity T: air temperature
u: horizontal component of wind w: vertical component of wind

with $a_E=1.1$ fits well the plotted points in the range $\zeta_v<-0.2$. The coefficient a_E is specificed by the value of $\sigma_q/|q_*|$ at $\zeta_v=-1$. Our value of a_E agrees well with the value obtained by Högström and Högström (1974) on an agricultural site. The value of $\sigma_q/|q_*|$ is about 2.2 at neutral stratification $\zeta_v=0$. The amount of data in the stable regime is inadequate to make definite statements about the behavior of $\sigma_q/|q^*|$ in that regime.

Fig. 21 (b) shows $\sigma_T/|T_*|$ plotted against ζ_v. This figure, compared with Fig. 21 (a), shows that $\sigma_T/|T_*|$ and $\sigma_q/|q_*|$ behaved similarly in the unstable regime. The ratio $\sigma_T/|T_*|$ showed a large scatter near neutral stratification, where both σ_T and T_* became small in magnitude.

Figs. 21 (c) and (d) show respectively σ_w/u_* and σ_u/u_* as a function of ζ_v. The ratio σ_w/u_* has value 1.2 to 1.3 at $\zeta_v=0$; it increases as ζ_v deviates from zero. The value of σ_u/u_* was larger than the value of σ_w/u_* within the stability range covered in this study. The standard deviation σ_u/u_* showed a large scatter. It is probable that this variability results partly from the inadequate sampling duration.

Correlation coefficient Figs. 22 (a) to (e) show the correlation coefficients plotted against the stability parameter ζ_v.

The correlation coefficient r_{wq} (Fig. 22 (a)) was positive in the range of $\zeta_v=-2.5$ to $+3$ that was covered in the present study. Its value is about 0.35 at $\zeta_v=0$. It increases with increasing instability up to 0.5 at $\zeta_v=-2.5$. It appears to decrease with increasing stability down to 0.2 at $\zeta_v=3$.

The correlation coefficient r_{wT} (Fig. 22 (b)) is positive in the unstable regime and increases with increasing instability. Its value attains 0.5 at $\zeta_v=-2.5$, the instability limit observed. In the unstable regime

$\zeta_v < -0.2$, r_{wT} (ζ_v) has a functional form similar to r_{wq} (ζ_v). The similarity collapses near neutral and in stable stratification. The value of r_{wT} decreases sharply as ζ_v approaches zero from negative ζ_v. It becomes negative near $\zeta_v=0$ at slightly postive ζ_v. The negative r_{wT} in the stable regime appears to be in the same order of magnitude as the positive r_{wT} in the unstable stratification. These results agree fairly well with those of Haugen et al. (1971) and McBean and Miyake (1972).

The correlation coefficient r_{wT} showed a large scatter in the near-neutral stratification where the involved quantities $\overline{w'T'}$ and σ_T become small.

The correlation coefficient r_{wu} (Fig. 22(c)) is consistently negative in the range of ζ_v examined in this experiment. Its magnitude $|r_{wu}|$ is about 0.3 near $\zeta_v=0$; it decreases with increasing instablility down to 0.1 at $\zeta_v=-2.5$.

The above results thus suggest a similarity between the transfer of water vapor and that of heat in the local free convection regime. Evidences provided by the experiments are summarized as follows. In the unstable stratification $\zeta_v < -0.2$, $\sigma_q/|q_*|$ and $\sigma_T/|T_*|$ vary as $(\zeta_v)^{-1/3}$, following the prediction for the local free convection regime. r_{wT} and r_{wq} increase while r_{wu} decreases with increasing instablility. In the fully developed unstable regime $\zeta_v \simeq -2.5$, r_{wq} has a large value of about 0.5 approximately equal to the value of r_{wT}.

Figs. 22 (d) and (e) show the correlation coefficients r_{u_1} and r_{uT} as a function of ζ_v. The sign of r_{u_1} is opposite to that of r_{wq} for any given value of ζ_v. This is expected since r_{wu} is definitely negative over the range of ζ_v covered in the present experiment. Both correlation coefficients r_{uq} and r_{uT} tend to decrease in magnitude with increasing instability.

Figs. 21 (a), (b) and Figs. 22 (a), (b) include the results obtained by Miyake and McBean (1970) over grass and the results obtained by Phelps and Pond (1971) over the sea. Their results, limited in stratification to near-neutral stability, are generally compatible with our results.

Spectrum

Two cases of spectrum analysis, one for an unstable stratification (09 h 42 m–57 m, September 18) and another for a near-neutral (slightly stable) statification (16 h 20 m–40 m, September 18) are described below. The turbulent fluctuations for these cases have been illustrated. The method of Tukey was used for spectrum computation. The sampling rate was 10 Hz.

Power spectrum Figs. 23 and 24 show the power spectra. The ordinate is (frequency) × (spectral density)/(variance) on a logarithmic

scale. The abscissa is frequency in Hz on a logarithmic scale. The spectra are presented without applying correction for the high frequency loss discussed above. Referring to the $-2/3$ power line that indicates the slope of spectrum in the inertial subrange, we see that the q-spectrum is significantly affected by the underestimate in high frequencies. Taking into account the resulting distortion in the q-spectrum, we can deduce some characteristics of the power spectra from the calculated results.

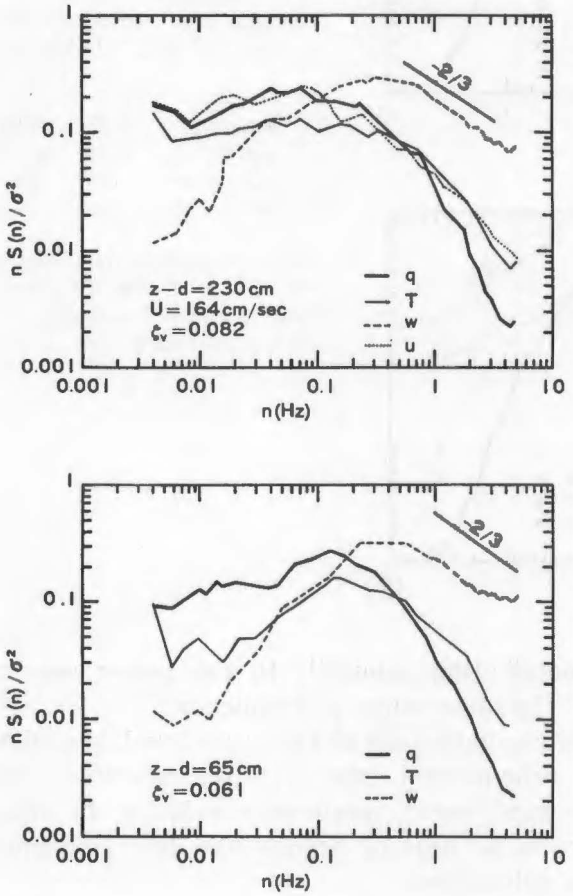

FIG. 23. Normalized power spectra $nS(n)/\sigma^2$ of specific humidity q, air temperature T, and vertical and horizontal components of wind, w and u. Near-neutral (slightly stable) case. 1620–1640 JST, Sept. 18, 1977, Hachihama.

$z-d$(cm)	230	65
σ_q^2(g/kg)^2	0.23	0.25
σ_T^2(°K)^2	0.07	0.13
σ_w^2(cm/s)^2	404	456
σ_u^2(cm/s)^2	490	—

In the near-neutral case (Fig. 23), q-spectrum displays roughly the same shape as T-spectrum. The spectrum of w is shifted toward higher frequencies relative to the spectra of T and q. Each spectrum shifts toward higher frequencies at the lower level.

In the unstable case (Fig. 24), the distinction of w-spectrum from q- or T-spectra become less marked compared with the near-neutral case. At the lower level, w-spectrum can be distinguished fairly well from other spectra. The distinction is almost obscured at the higher

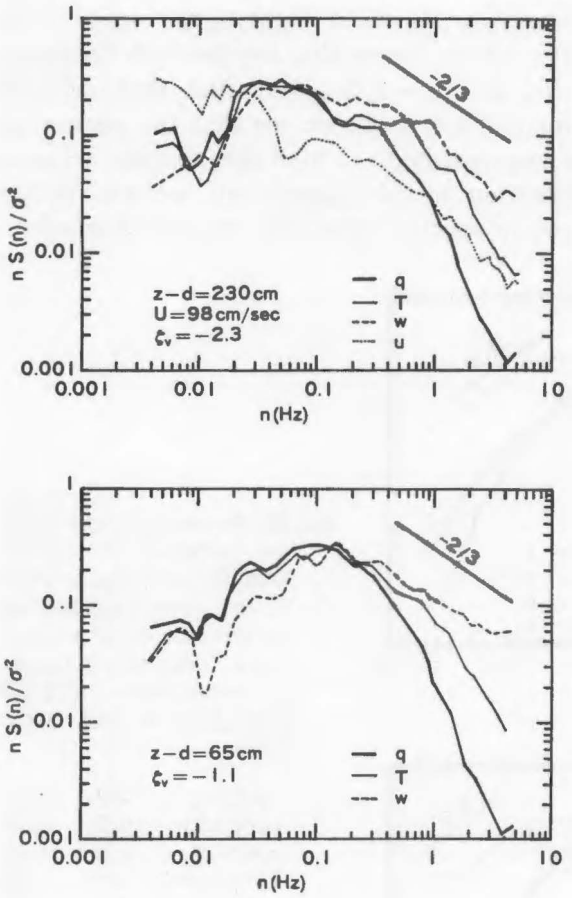

FIG. 24. Normalized power spectra $nS(n)/\sigma^2$ for an unstable case. 0942-0957 JST, Sept. 18, 1977, Hachihama.

z-d(cm)	230	65
σ_q^2(g/kg)^2	0.27	0.58
σ_T^2(°K)^2	0.33	0.60
σ_w^2(cm/s)^2	435	633
σ_u^2(cm/s)^2	1118	—

Dip at about 0.01 Hz adjointed by rise on the low frequency side is ascribed to inadequacy of the averaging time.

level, and the frequencies contributing primarily to the power spectra of w, T and q span broadly the same range of frequency.

The u-spectrum, which is available only at the upper level, is similar to q- or T-spectra in the near-neutral case. In the unstable case, the u-spectrum is shifted toward lower frequencies relative to other spectra, and its peak appears to lie near or beyond the low frequency limit attained in the present calculation.

Cospectrum Figs. 25 and 26 show the w-q and w-T cospectra for the near-neutral case and for the unstable case, respectively. The ordinate is (frequency) × (cospectral density)/(covariance) on a linear scale. The abscissa is the frequency in Hz on a logarithmic scale. Thus, the area between the spectrum curve and the abscissa is proportional to the spectral contribution to the covariance.

The calculated cospectra are distorted by high frequency loss arising from the averaging effect of the sensors. In particular, the sharp peak and the steep fall on the high frequency side are spuriously exaggerated

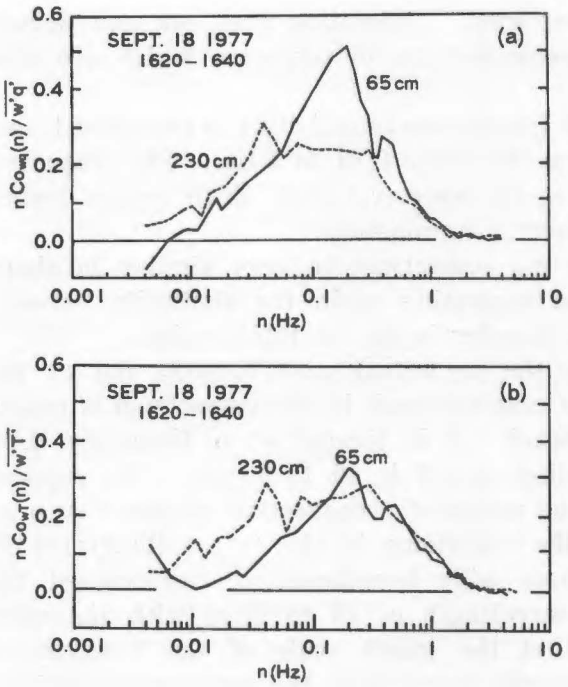

FIG. 25. Normalized cospectra of w-q and w-T for a near-neutral (slightly stable) case.

z-d (cm)	230	65
$\overline{w'q'}$(g/kg·cm/s)	3.58	2.95
$\overline{w'T'}$(°K cm/s)	−1.71	−3.18

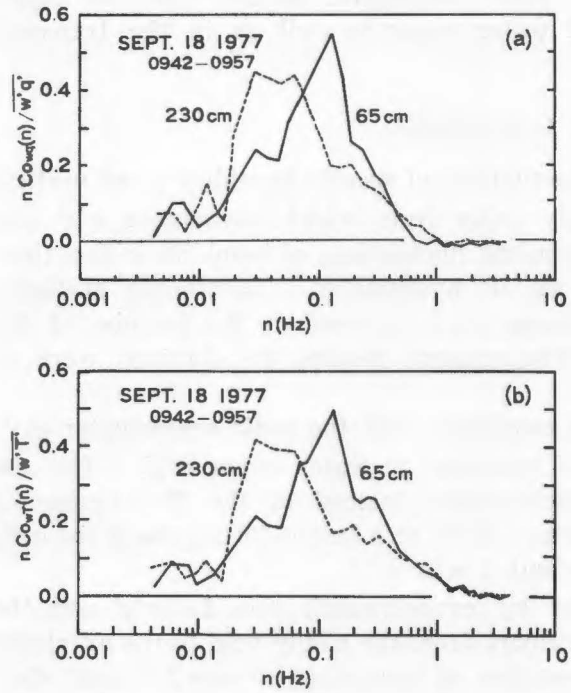

FIG. 26. Normalized cospectra of w-q and w-T for an unstable case.

z-d (cm)	230	65
$\overline{w'q'}$(g/kg·cm/s)	5.33	7.86
$\overline{w'T'}$(°K cm/s)	5.44	9.16

for the cospectra at the lower level. Admitting that, we can deduce from the calculated results some features of cospectra which are considered to be significant.

Figs. 25 and 26 show that frequencies contributing to turbulent transport are limited practically to the range 0.01 to 1 Hz. The frequency of maximum contribution, i. e., the cospectral peak, shifts toward higher frequencies as the crop surface is approached.

In the unstable case the w-q cospectrum is very similar in shape to the w-T cospectrum, thus suggesting again the similarity between the heat transfer and vapor transfer in the unstable regime.

In the near-neutral case the cospectral peak becomes flat at the upper level. In the unstable case the peak in the cospectrum is rather sharp even at the upper level. It is located at a frequency 0.02 to 0.07 Hz. The corresponding period is 15 to 50 sec. We suppose that this period represents the period of "convective plumes" such as indicated by the saw-tooth-like variations in the traces illustrated in Fig. 16. Using Taylor's frozen eddy hypothesis, we can convert the period 15 to 50 sec into a wavelength of 15 to 50 m with the wind velocity $\simeq$ 1 m/s. We see that the length scale of the "convective plume" is one order of magnitude larger than the measurement height. These values are in fairly good agreement with values obtained by Monji (1973) for the heat transfer on an extensive salt field. We presume that in much unstable cases, such "convective plumes" play an important part in the transport of water vapor as well as in the transport of heat.

CONCLUSIONS

We measured turbulent fluctuations of specific humidity q and vertical wind component w over paddy fields from which covariance $\overline{w'q'}$ was evaluated. We measured turbulent fluctuations of humidity with a thermocouple psychrometer and an IR hygrometer. Turbulence statistics involved in the transport process were analyzed on the premise of the Monin-Obukhov similarity. The primary results we obtained were as follows.

1) The IR hygrometer combined with the sonic anemometer gave reasonably accurate values of transport of water vapor $\overline{w'q'}$. The use of fine-wire thermocouple psychrometer instead of the IR hygrometer led to an underestimate of about 20 % at a height 20 cm above the crop surface for wind speeds of about 1 m/s.

2) Latent heat transfer by evapotranspiration $L\rho\ \overline{w'q'}$ was the major component in heat transport from the paddy field to the overlying air. The daytime total evaporation on September 18 was 2.6 mm. Cor-

rected for the underestimate mentioned above, this value approximates the value obtained from the heat balance at a similar crop growth stage.

3) In the unstable regime $\zeta_v < -0.2$, the normalized variance of humidity $\sigma_q/|q_*|$ varied as $(-\zeta_v)^{-1/3}$, following the prediction of the similarity theory for local free covection regime. The functional form of $\sigma_q/|q_*|$ (ζ_v) is almost identical with that of $\sigma_T/|T_*|$ (ζ_v) in this regime. The correlation coefficients r_{wq} and r_{wT} increase with increasing instability in a very similar way.

4) In the near-neutral stratification, r_{wT} approaches zero and becomes negative in stable stratification, while r_{wq} continues to be positive. This corresponds to the fact that over paddy fields temperature inversion occurred in mid- or late afternoon while evapotranspiration continued after sunset.

5) The cospectrum between w and q, multiplied by frequency, shows a well defined peak at about 0.1 Hz near the crop surface. As the measuring height is raised, the frequency range contributing to the covariance shifts to the lower frequency, and the spectral peak tends to be flattened.

6) In the unstable case the frequencies contributing substantially to the w-q cospectrum are restricted within a relatively narrow range and the frequency of the spectral peak is still easy to identify at a height about 2 m above the crop. For the example given, the peak frequency was 0.02 to 0.07 Hz at $z-d=230$ cm. The corresponding period is 15 to 50 sec and the scale of the eddies is 15 to 50 m. This period is of the same order as the period of the "convective plumes" noted in the fine records of the fluctuations of w, T_a and T_w.

Acknowledgements We are grateful to Prof. K. Sahashi and Dr. T. Maitani for their discussions during the course of this work and to Misses N. Hiraoka for her continued assistance in preparation of the manuscript. Thanks are also due to Dr. Y. Miyake who permitted us to use the experimental site on the University Farm.

REFERENCES

Busch, N. E. 1973. On the mechanism of atmospheric turbulence. Workshop on Micrometeorology, D. A. Haugen, editor. Amer. Met. Soc. 1-65.

Haugen, D. A., Kaimal, J. C. and Bradley, E. F. 1971. An experimental study of Reynolds stress and heat flux in the atmospheric surface layer. Quart. J. R. Met. Soc. 97 : 168–180.

Högström, U. and Högström, A. S. 1974. Turbulence mechanism at an agricultural site. Boundary-Layer Met. 7 : 373–389.

Kaimal, J. C. and Businger, J. A. 1970. Case studies of a convective plume and a dust devil. J. Appl. Met. 9 : 612–620.

Kaimal, J. C., Wyngaard J. C. and Haugen, D. A. 1968. Deriving power spectra from a

three component sonic anemometer. J. Appl. Met. 7 : 827–837.
McBean, G. A. and Miyake, M. 1972. Turbulent transfer mechanisms in the atmospheric surface layer. Quart. J. R. Met. Soc. 98 : 383–398.
Mitsuta, Y., Mori, Y., Fujitani, T. and Hanafusa, T. 1973. On the definitions of mean wind speed and direction. Annals of Disaster Prevention Research Institute, Kyoto University. 16 B : 319–326.
Miyake, M. and McBean, G. A. 1970. On the measurement of vertical humidity transport over land. Boundary-Layer Met. 1 : 88–101.
Monji, N. 1973. Budgets of turbulent energy and temperature variance in the transition zone from forced to free convection. J. Meteor. Soc. Japan. 51 : 133–145.
Ohtaki, E. and Seo, T. 1976. Infrared device for measurement of carbon dioxide fluctuations under field conditions. II. Double beam system. Ber. Ohara Inst. landw. Biol. Okayama Univ. 16 : 183–190.
Pasquill, F. 1974. Atmospheric Diffusion, 2nd ed., Horwood, Chichester.
Phelps, G. T. and Pond, S. 1971. Spectra of the temperature and humidity fluctuations and the fluxes of moisture and sensible heat in the marine boundary layer. J. Atmos. Sci. 28 : 918–928.
Sano, Y. and Mitsuta, Y. 1968. Dynamic response of the hygrometer using fine thermocouple psychrometer. Special Contributions of Geophysical Inst., Kyoto Univ. 8 : 61–70.
Seo, T. and Ohtaki, E. 1976. Infrared device for measurement of carbon dioxide fluctuations under field conditions. III. Adaptation to infrared hygrometry. Ber. Ohara Inst. landw. Biol. Okayama Univ. 16 : 191–198.
Seo, T. and Yamaguchi, N. 1968. A note on the evapotranspiration from a paddy field. Ber. Ohara Inst. landw. Biol. Okayama Univ. 14 : 133–143.
Silverman, B. A., 1968. The effect of spatial averaging on spectrum estimation. J. Appl. Met. 7 : 168–172.
Taylor, R. J. 1963. Effects of instrumental inertia on measurement of the turbulent flux of water vapor. Aust. J. Appl. Sci. 14 : 27–37.
Webb, E. K. 1965. Aerial Microclimate. Meteorological Monographs published by the American Meteor. Soc. Vol. 6, No. 28 : Agricultural Meteorology. Chap. 2.